iScience

CellPress
OPEN ACCESS

Article

Region-specific sympatho-adrenergic regulation of specialized vasculature in bone homeostasis and regeneration

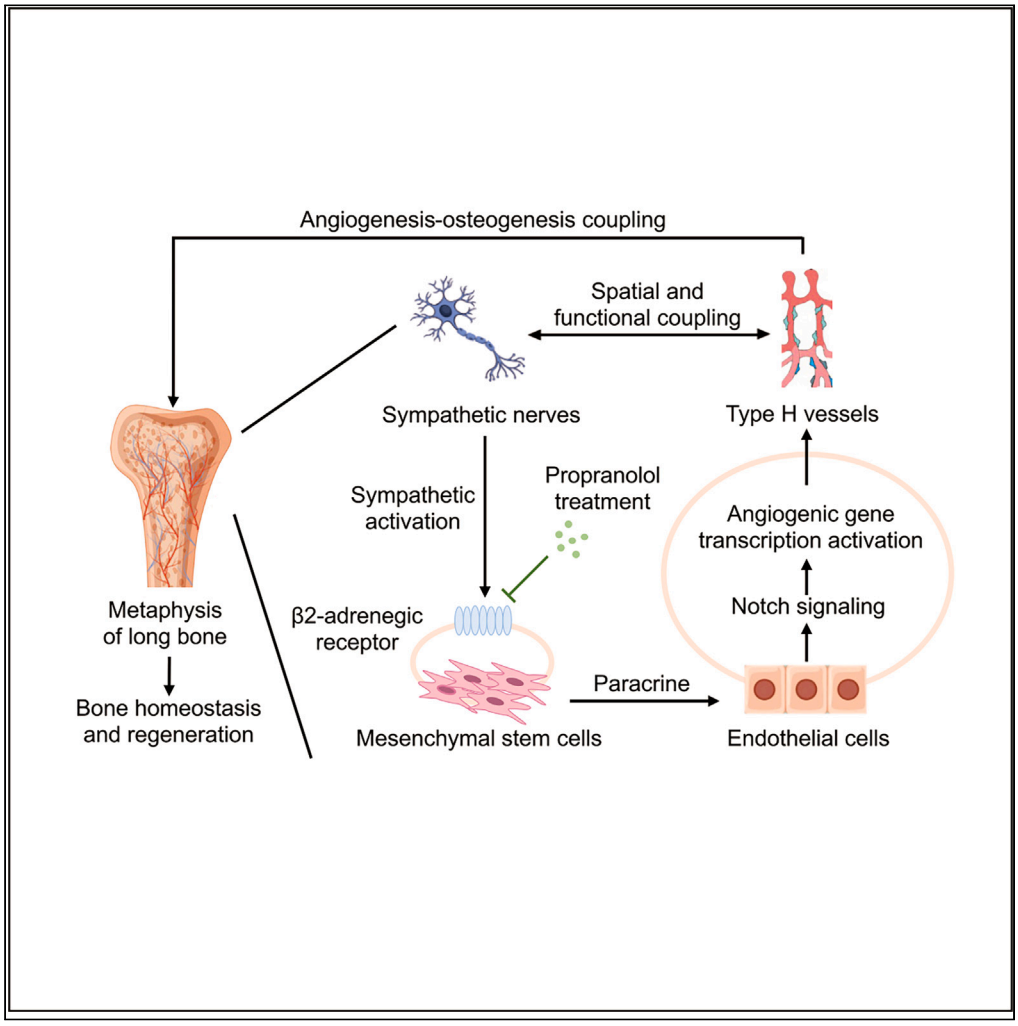

Hao-Kun Xu, Jie-Xi Liu, Chen-Xi Zheng, ..., Liang Kong, Yong-Jin Chen, Bing-Dong Sui

liangkong2014@163.com (L.K.)
13991979822@139.com (Y.-J.C.)
bingdong@fmmu.edu.cn (B.-D.S.)

Highlights

Sympathetic nerves spatially and functionally correlate with type H vessels in bone

Sympathoexcitation regulates type H vessel formation and bone mass maintenance

Sympathetic cues regulate angiogenic signaling via an MSC-EC paracrine mode

Pharmacological ADRB inhibition protects type H vessels and bone mass in OVX

Xu et al., iScience *26*, 107455
September 15, 2023
https://doi.org/10.1016/j.isci.2023.107455

iScience

CellPress
OPEN ACCESS

Article

Region-specific sympatho-adrenergic regulation of specialized vasculature in bone homeostasis and regeneration

Hao-Kun Xu,[1,2,7] Jie-Xi Liu,[1,7] Chen-Xi Zheng,[1,7] Lu Liu,[1,3] Chao Ma,[1] Jiong-Yi Tian,[1] Yuan Yuan,[1,4] Yuan Cao,[1,3] Shu-Juan Xing,[1] Si-Ying Liu,[3] Qiang Li,[5] Ya-Juan Zhao,[5] Liang Kong,[6,*] Yong-Jin Chen,[5,*] and Bing-Dong Sui[1,8,*]

SUMMARY

Type H vessels couple angiogenesis with osteogenesis, while sympathetic cues regulate vascular and skeletal function. The crosstalk between sympathetic nerves and type H vessels in bone remains unclear. Here, we first identify close spatial connections between sympathetic nerves and type H vessels in bone, particularly in metaphysis. Sympathoexcitation, mimicked by isoproterenol (ISO) injection, reduces type H vessels and bone mass. Conversely, beta-2-adrenergic receptor (ADRB2) deficiency maintains type H vessels and bone mass in the physiological condition. *In vitro* experiments reveal indirect sympathetic modulation of angiogenesis via paracrine effects of mesenchymal stem cells (MSCs), which alter the transcription of multiple angiogenic genes in endothelial cells (ECs). Furthermore, Notch signaling in ECs underlies sympathoexcitation-regulated type H vessel formation, impacting osteogenesis and bone mass. Finally, propranolol (PRO) inhibits beta-adrenergic activity and protects type H vessels and bone mass against estrogen deficiency. These findings unravel the specialized neurovascular coupling in bone homeostasis and regeneration.

INTRODUCTION

Over the past decades, extensive research has established the intricate connection between the nervous system and the vasculature. It has become evident that the nervous system plays a crucial role in maintaining vascular homeostasis and regulating the physiological function of blood vessels.[1–3] In the central nervous system (CNS), the neurovascular unit (NVU) comprising neurons, astrocytes, and vascular smooth muscle has emerged as a pivotal regulatory structure for blood vessels. Conversely, in the peripheral nervous system (PNS), neural regulation of blood vessels primarily occurs via the secretion of neurotransmitters.[4–6] Of particular importance in the PNS is the sympathetic nervous system (SNS), which releases various vasoactive mediators, including norepinephrine/noradrenaline (NE/NA), to regulate vasoconstriction and blood pressure.[7,8] This vascular effect of sympathoexcitation is predominantly mediated by adrenergic receptors (ADRs) expressed in smooth muscle cells, the principal cells involved in vascular wall formation.[9,10] As another essential component of the vasculature, the endothelium has also been reported to be regulated by the SNS, either indirectly or directly. Indirectly, SNS-induced smooth muscle contractions trigger the release of signaling molecules from ECs, which in turn mediate endothelium-dependent anticontractile responses.[11] Alternatively, the SNS directly activates ADRs expressed in ECs, leading to the release of nitric oxide (NO), regulation of vascular contraction, and overall endothelial function.[12] Among the various ADRs, the activation of the alpha-adrenergic receptor (ADRA) has been implicated in endothelial dysfunction characterized by increased leukocyte adhesion to ECs, vascular inflammation and vascular permeability.[13–15] Activation of the beta-1-adrenergic receptor (ADRB1) has been associated with arterial endothelial injury.[16] Activation of beta-2-adrenergic receptor (ADRB2) has been shown to promote NO release and vascular contraction which is opposite to that of ADRA.[17,18] In addition, the ADRB2 activation has been demonstrated to promote the proliferation, migration, and differentiation of endothelial progenitor cells (EPCs) which is essential for vasculogenesis during embryonic development.[19,20] However, in the postnatal tissues, whether and how the mature endothelium responds to sympathoexcitation through ADRB2 activation and regulates angiogenesis remains unclear.

[1]State Key Laboratory of Military Stomatology & National Clinical Research Center for Oral Diseases & Shaanxi International Joint Research Center for Oral Diseases, Center for Tissue Engineering, School of Stomatology, The Fourth Military Medical University, Xi'an, Shaanxi 710032, China

[2]Department of Oral Anatomy and Physiology, School of Stomatology, The Fourth Military Medical University, Xi'an, Shaanxi 710032, China

[3]Department of Orthodontics, School of Stomatology, The Fourth Military Medical University, Xi'an, Shaanxi 710032, China

[4]Exercise Immunology Center, Wuhan Sports University, Wuhan, Hubei 430079, China

[5]Department of General Dentistry & Emergency, School of Stomatology, The Fourth Military Medical University, Xi'an, Shaanxi 710032, China

[6]Department of Oral and Maxillofacial Surgery, School of Stomatology, The Fourth Military Medical University, Xi'an, Shaanxi 710032, China

[7]These authors contributed equally

[8]Lead contact

*Correspondence: liangkong2014@163.com (L.K.), 13991979822@139.com (Y.-J.C.), bingdong@fmmu.edu.cn (B.-D.S.)

https://doi.org/10.1016/j.isci.2023.107455

In the mammalian skeletal system, the neural and vascular networks are densely distributed and are crucial in governing bone formation and remodeling.[21] Particularly, the autonomic nervous system, through sympathetic and parasympathetic pathways, regulates bone formation, homeostasis, and remodeling.[21] The neurotransmitters released from active sympathetic nerves are recognized by ADRBs that have been identified as a critical messenger mediator linking the brain to the skeleton since the early 2000s.[22–26] In the context of bone, the three different ADRB receptors exert diverse functions. ADRB1 primarily regulates bone metabolism, exerting an anabolic stimulus during growth and development, and in response to mechanical stimulation.[27–29] In contrast, ADRB2 signaling predominantly suppresses bone formation, leading to bone pathologies and decreased bone mass.[22,27] ADRB3 plays a limited role in bone regulation, primarily influencing hematopoiesis rather than bone remodeling.[29–32] Additionally, the vasculature, as an integral component of the bone remodeling unit, is critical for bone homeostasis by providing nutrient transport, delivering immune cells and supporting hematopoiesis.[21,33] Notably, recent evidence has highlighted the remarkable morphological and functional heterogeneity of ECs in local microenvironments.[34] Specifically, type H endothelium that can give rise to type L endothelium has been discovered as a specific vessel subtype coupling angiogenesis with osteogenesis in bone.[35,36] However, the relationship between sympathetic nerves and type H vessels and its implications for bone physiology remains unclear. Thus, it is of great significance to uncover the effects and underlying mechanisms of the specialized nerve-vessel crosstalk in bone homeostasis and regeneration.

In this study, we demonstrate the close spatial distribution of the sympathetic nerves and type H vessels in bone, especially in the metaphysis region. The sympathetic activation induced by isoproterenol (ISO) injection led to type H vessel injury and bone loss. Conversely, in physiological conditions, deficiency of ADRB2 resulted in the restoration of type H vessels and bone mass. *In vitro* experiments were performed to evaluate the direct regulatory effect of sympathetic signal on ECs or indirectly through paracrine action of mesenchymal stem cells (MSCs), the latter of which was proved to be critical and induced alterations of expression of multiple angiogenic factors in ECs. Mechanistically, the Notch signaling in ECs was revealed to underlie the sympathoexcitation-governed type H vessel formation, and corresponding effects on osteogenesis contributed to the regulation of bone mass. Moreover, ADRB inhibition by propranolol (PRO) was proved to protect type H vessels and maintain bone mass in the estrogen-deficient pathological condition. Overall, our study confirms the close spatial and functional relationship between sympathetic nerves and type H vessels in bone under both physiological and pathological conditions, emphasizing the significance of specialized neurovascular coupling in maintaining bone homeostasis and supporting bone regeneration.

RESULTS

Sympathetic nerves are spatially coupled with type H vessels in bone

To investigate the relationship between sympathetic nerves and specialized vessels, at the beginning of this study, we particularly investigated the distribution of sympathetic nerves (marked by tyrosine hydroxylase, TH), $CD31^{hi}EMCN^{hi}$ vessels (Type H vessels) and $CD31^{lo}EMCN^{lo}$ vessels (Type L vessels) in femurs (Figures 1A and 1B). Immunofluorescent staining revealed a correlation between the distribution of sympathetic nerves and type H vessels rather than single $CD31^{hi}$ or $EMCN^{hi}$ vessels in both metaphysis and diaphysis (Figures 1A and 1B). Our observations align with previous literature, showing the presence of TH^+ cells in the metaphysis, diaphysis, and periosteum.[37,38] In the metaphysis, TH^+ cells predominantly exist as free nerve endings and were demonstrated to be distributed closely with type H vessels, as also shown in regional magnification (Figure 1A). While in the diaphysis and periosteum, sympathetic nerve fibers in addition to free nerve endings were observed around blood vessels marked with CD31 rather than specifically associated with type H vessels, as also shown in regional magnification (Figure 1B). Based on the predominant distribution of type H and L vessels in the metaphysis and diaphysis, we conducted quantitative analyses of TH^+ cells in these areas (Figures 1C–1E). The specific criteria for analyzing the regions of interest (ROIs) are illustrated (Figures S1A–S1C). Quantification analysis confirmed that sympathetic nerves were overlapped or adjacent to type H vessels (Figure 1C), and this distribution pattern was particularly prominent in the metaphysis. Although the percentage of sympathetic nerves-correlated type H vessels was higher than type L vessels compared between the Type H group and the Type L group in both metaphysis and diaphysis, this distribution pattern is more pronounced in the metaphysis compared between the Type H group in the metaphysis and the Type H group in the diaphysis (Figure 1D). Moreover, the percentage of type H vessel-correlated sympathetic nerves was also higher than that of type L vessel-correlated sympathetic nerves in the metaphysis (Figure 1E), indicating a close spatial relationship between sympathetic nerves and type H vessels. Notably, as the close association between TH^+ sympathetic nerves and type

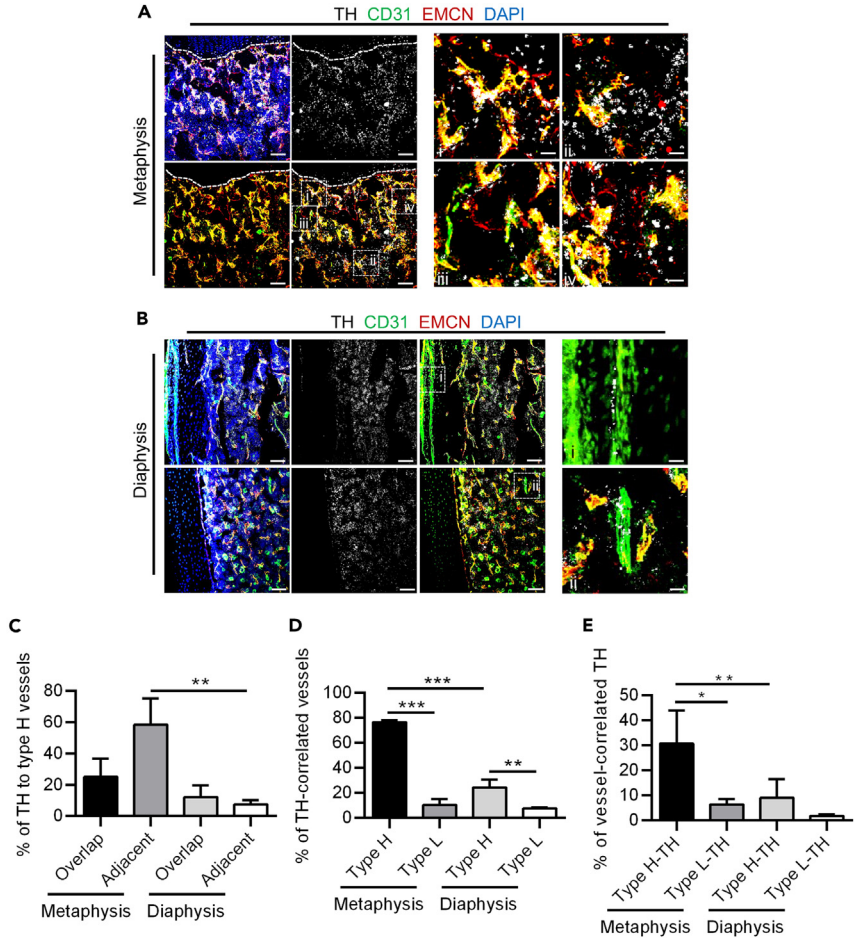

Figure 1. Sympathetic nerves are spatially coupled with type H vessels in bone

(A) TH (white), CD31 (green) and EMCN (red) co-immunostaining at metaphysis in femurs, counterstained by DAPI (blue). Dashed lines indicate the margin of growth plates. Scale bars, 100 μm i-iv, enlarged regions. Scale bars, 20 μm.

(B) TH (white), CD31 (green) and EMCN (red) co-immunostaining at diaphysis in femurs, counterstained by DAPI (blue). Scale bars, 100 μm i-ii, enlarged regions. Scale bars, 20 μm.

(C) Quantification of sympathetic nerves overlapped or adjacent to type H vessels (%). $N = 3$ per group.

(D) Quantification of sympathetic nerves-correlated vessels (%). $N = 3$ per group.

(E) Quantification of vessel-correlated sympathetic nerves (%). $N = 3$ per group.

Data represent mean ± SD. Statistical analysis is performed by Student's *t* test for two-group comparison or by one-way analysis of variance followed by Newman–Keuls post-hoc tests for multiple comparisons. *, $p < 0.05$; **, $p < 0.01$; ***, $p < 0.001$.

H vessels is especially prominent in the metaphysis, and given the important role of the metaphysis in bone homeostasis maintenance and regeneration,[37] we focused on the metaphysis in further experiments.

Sympathoexcitation impaired type H vessels and resulted in osteopenia

To investigate the effect of sympathetic activation on type H vessels and bone mass, the model of sympathetic activation was established by administering continuous daily intraperitoneal injections of the ADRB agonist ISO for four weeks (Figure S2A). We evaluated the impact of sympathetic activation by examining bone mass and type H vessel density (Figure S2A). Micro-CT technology was used to examine the mouse femurs, and the results showed a significant decrease in both trabecular and cortical bone in the ISO group compared to the PBS group (Figures 2A and 2B). Further analysis of the parameters such as trabecular bone volume over tissue volume (Tb.BV/TV), trabecular thickness (Tb.Th), trabecular separation (Tb.Sp), and trabecular number (Tb.N) for the trabecular bone (Figures 2C–2F), as well as the cortical area (Ct.Ar) and cortical thickness (Ct.Th) for the cortical bone (Figures 2G and 2H), confirmed the bone phenotypic

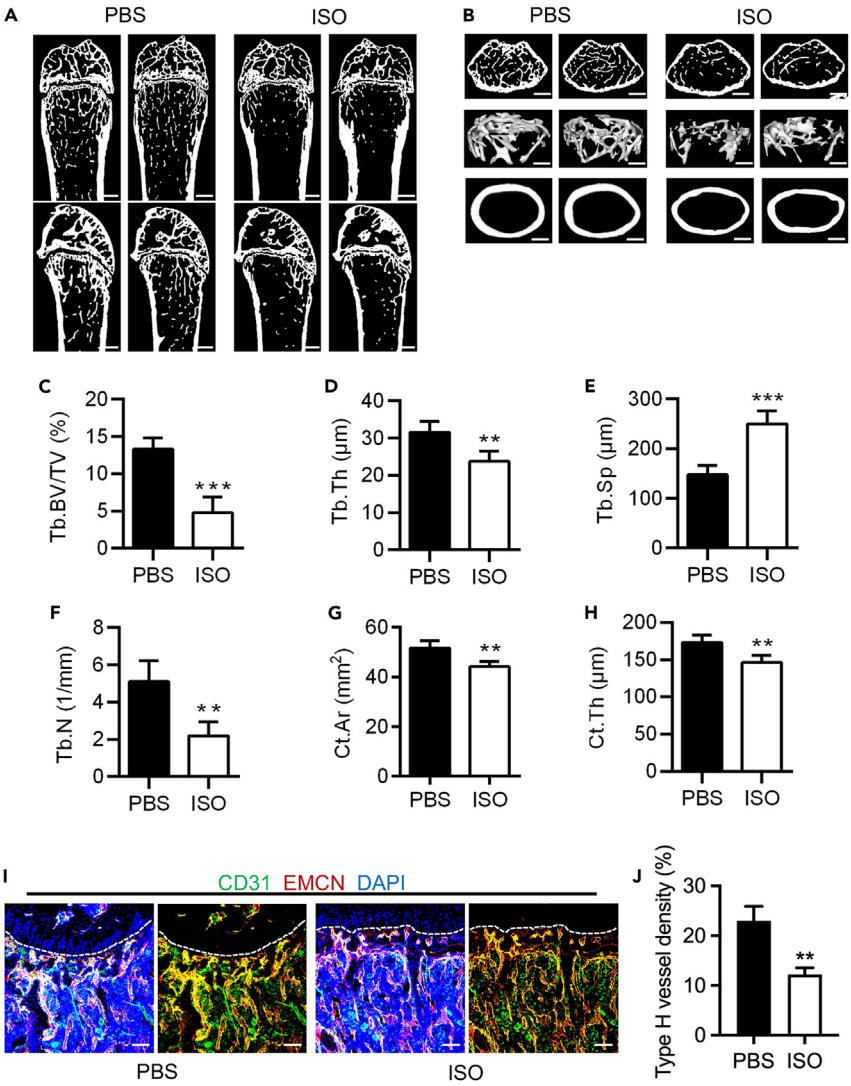

Figure 2. Sympathoexcitation impaired type H vessels and resulted in osteopenia

(A and B) Micro-CT analysis and 3D views of femurs of mice treated with PBS and ISO. ISO was injected intraperitoneally for 4 weeks. Scale bars, 500 μm (A) and 250 μm (B).

(C–F) Parameter analysis of trabecular bone mass. Tb.BV/TV, trabecular bone volume over tissue volume; Tb.Th, trabecular thickness; Tb.Sp, trabecular separation; Tb.N, trabecular number. *N* = 4 per group.

(G and H) Parameter analysis of cortical bone mass. Ct.Ar, cortical bone area; Ct.Th, cortical bone thickness. *N* = 4 per group.

(I) CD31 (green) and EMCN (red) co-immunostaining at metaphysis of mice treated with PBS and ISO, counterstained by DAPI (blue). Scale bar, 100 μm.

(J) Quantification of type H vessel density (%). *N* = 3 per group.

Data represent mean ± SD. Statistical analysis is performed by Student's *t* test. **, $p < 0.01$; ***, $p < 0.001$.

changes. Additionally, fluorescent labeling techniques were employed to label type H vessels at the metaphysis, and a comparison of type H vessel density between the ISO group and the PBS group was performed. Fluorescent images and statistical analysis revealed a lower density of type H vessels in the ISO group compared to the PBS group (Figures 2I and 2J). Overall, our findings indicate that the mimic of sympathetic activation through ISO injection leads to type H vessel decrease and bone loss.

ADRB2 deficiency maintained type H vessels in bone mass accrual

Next, we intended to further confirm the significance of sympathetic regulation of type H vessels in bone physiology. In our previous findings, we showed that type H vessels reduce from mouse adolescence to

adulthood.[39] Accordingly, we used *Adrb2*$^{-/-}$ mice as described[27] and measured the density of type H vessels and bone mass in the femurs of mice during the physiological bone mass accrual process. Immunofluorescent staining revealed that the type H vessel density of 4, 8, and 12 weeks *Adrb2*$^{-/-}$ mice was higher than wild-type (WT) mice at paired age (Figure 3A). Further quantitative analysis confirmed that the density of type H vessels in WT mice gradually decreased with age (Figure 3B). Although that type H vessels in *Adrb2*$^{-/-}$ mice seemed to also decline with age, there was no statistical significance among groups (Figure 3C). Furthermore, 8- and 12-week-old, *Adrb2*$^{-/-}$ mice demonstrated higher levels of type H vessel density compared to WT mice (Figure 3D). These findings suggest that the deficiency of ADRB2 mitigates the age-related decrease in type H vessels. Micro-CT analysis showed the corresponding bone mass changes with type H vessel maintenance because the bone mass of *Adrb2*$^{-/-}$ mice was also preserved in 8 weeks compared with age-paired WT mice in both trabecular and cortical bone (Figures 3E and 3F), confirmed by statistical analysis of the corresponding parameters of Tb.Th and Cr.Ar (Figures 3G–3L). These findings provide evidence supporting the pivotal role of ADRB2 in mediating the physiological regulation of type H vessels and bone mass by sympathetic nerves.

Sympathoexcitation regulated angiogenesis through a paracrine mode and at the gene transcription level

To investigate the mechanism of sympathoexcitation regulating type H vessels, we next conducted *in vitro* experiments of angiogenesis regulation. It has been reported that capillaries are composed of ECs supported by pericytes, which refer to a collective term for cells located around blood vessels encompassing various cell types, including MSCs with a regulatory role in angiogenesis.[40,41] Thus, we included both ECs and MSCs that could potentially contribute to the regulation of EC function in our further experiments. Firstly, considering the close spatial relationship between sympathetic nerves and blood vessels, we detected the protein expression of ADRB1/2/3 in both human- and mouse-derived MSCs and ECs. The results showed the presence of all three beta-adrenergic receptors in both MSCs and ECs in humans and mice (Figures S3A–S3C and S4A–S4C). To mitigate the risk of non-specific antibody binding, we further evaluated the mRNA expression of these ADRBs in MSCs and ECs from both species. The analysis confirmed the expression of all three ADRB mRNAs in the included samples (Figures S3D, S3F, S4D, and S4F), suggesting the possible response to sympathetic stimulation of both MSCs and ECs.

Secondly, we examined whether sympathetic cues directly regulated ECs or indirectly through MSCs. We treated ECs with ISO or with the supernatant of ISO-pretreated MSCs and evaluated their tube forming ability (Figures S5A and S5B). Notably, we used human-derived MSCs and ECs to provide clinical relevance in this section, which is also acceptable in supporting the angiogenic research *in vivo*.[42,43] Results showed that direct treatment of ECs with ISO did not have a significant inhibitory effect on their tube formation, while indirect treatment of ECs with the supernatant of ISO-conditioned MSCs substantially inhibited their tube formation (Figures S5A and S5B). Based on the analysis parameters provided (Figure S6), we have conducted statistical analysis on parameters related to junctions and branches. The quantitative analysis further revealed that direct ISO treatment of ECs did not lead to a decrease in "junction/per field" and "ratio of branching length" compared to the control group (Figures S5C and S5D). In contrast, indirect ISO treatment via MSCs significantly inhibited the formation of junctions and branches of ECs (Figures S5E and S5F). These results suggested that the sympathetic regulation of EC angiogenesis is through the paracrine effect of MSCs rather than the direct response of ECs.

Lately, to further investigate the mechanism by which ISO indirectly regulated EC angiogenesis through MSCs, we performed the analysis at the transcription levels of angiogenesis-related genes (*VEGF*, *BFGF*, *PDGFB*, *ANG1*, and *ANG2*) in human-derived MSCs and ECs after different modes of ISO treatment (Figures S7A–S7E). The results revealed a decrease in mRNA levels of *VEGF*, *BFGF*, *PDGFB*, and *ANG1* after direct ISO treatment (Figures S7A–S7D). However, there were no significant changes in the mRNA levels of *ANG2* after direct ISO treatment (Figure S7E). In contrast, after indirect ISO treatment of ECs through MSCs, all five angiogenesis-related genes exhibited a significant decrease in mRNA levels, and the extent of mRNA level reduction was more remarkable than that in the direct group (Figures S7A–S7E). Furthermore, based on our previous findings indicating that the Notch signaling contributes to the formation of type H vessels,[44] we examined the expression of NICD, the active component of the Notch pathway, in ECs (Figure S7F). The results demonstrated a significant reduction in NICD expression after indirect ISO treatment of ECs through MSCs (Figure S7F). These data suggested that under indirect treatment with ISO, the paracrine effects of MSCs importantly regulated the angiogenic gene expression of ECs possibly

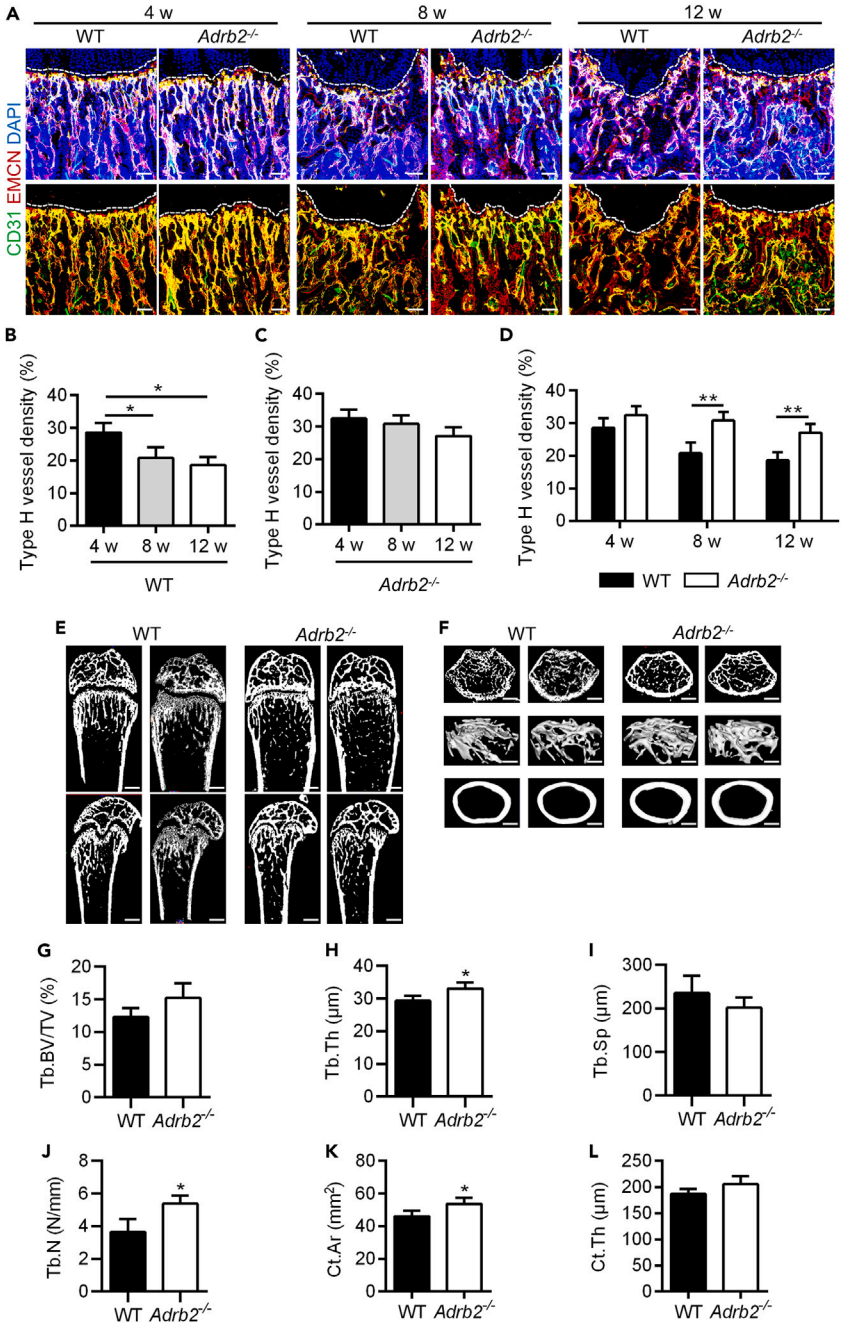

Figure 3. ADRB2 deficiency maintained type H vessels in bone mass accrual

(A) CD31 (green) and EMCN (red) co-immunostaining at metaphysis of WT and *Adrb2*$^{-/-}$ mice at 4, 8, and 12 weeks, counterstained by DAPI (blue). Scale bar, 100 μm.

(B) Quantification of type H vessels density (%) in WT mice at 4/8/12 w. *N* = 3 per group.

(C) Quantification of type H vessels density (%) in *Adrb2*$^{-/-}$ mice at 4/8/12 w. *N* = 3 per group.

(D) Quantification of type H vessels density (%) in WT mice and *Adrb2*$^{-/-}$ mice at 4/8/12 w.

(E and F) Micro-CT analysis and 3D views of femurs of WT and *Adrb2*$^{-/-}$ mice at 8 w. Scale bars, 500 μm (E) and 250 μm (F).

(G–J) Parameter analysis of trabecular bone mass. Tb.BV/TV, trabecular bone volume over tissue volume; Tb.Th, trabecular thickness; Tb.Sp, trabecular separation; Tb.N, trabecular number. *N* = 4 per group.

(K and L) Parameter analysis of cortical bone mass. Ct.Ar, cortical bone area; Ct.Th, cortical bone thickness. *N* = 4 per group.

Figure 3. *Continued*
Data represent mean ± SD. Statistical analysis is performed by Student's *t* test for two-group comparison, by one-way analysis of variance followed by Newman–Keuls post-hoc tests for multiple comparisons, or by two-way analysis of variance followed by Sidak's tests for multiple comparisons. *, $p < 0.05$; **, $p < 0.01$.

in related to Notch signaling alterations. These findings reflected the adaptability and responsiveness of ECs under sympathetic cues and implied that ECs undergo genetically programmed changes after indirect treatment with ISO.

Sympathoexcitation regulated type H vessel formation attributing to Notch signaling and governed bone mass through the angiogenesis-osteogenesis coupling

Next, we further investigated the *in vivo* mechanism underlying sympathetic regulation of the formation and maintenance of type H vessels. Immunofluorescence staining was conducted in the above mouse models, including ISO-mimicked sympathoexcitation and ADRB2 deficiency, to examine $NICD^+$ cell expression in the metaphysis (Figures 4A and 4C). Quantification analyses were further conducted to calculate the $NICD^+$ type H vessel density in the two models, and the specific criteria of ROIs for quantification of $NICD^+$ type H vessels are shown (Figure S1D). Statistical analysis revealed a significant decrease in $NICD^+$ type H vessel density in the ISO group compared to the PBS group (Figure 4B). In the ADRB2 deficiency model, the density of $NICD^+$ type H vessels was noticeably higher compared to WT (Figure 4D). These results indicate that ISO, acting as an ADRB agonist, exerts a negative effect, while the deficiency of ADRB2 provides a protective effect on type H vessels in bone possibly attributing to changes of the Notch pathway.

Taking into consideration the coupling of type H vessel formation and osteogenesis, we further conducted immunofluorescence staining to label $RUNX2^+$ cells in the metaphysis of both models of sympathetic regulation (Figures 5A–5D). In the ISO model, a significant decrease in $RUNX2^+$ cell density was observed and quantified in the ISO group compared to the PBS group (Figures 5A and 5B). On the contrary, ADRB2 deficiency maintained a significantly higher density of $RUNX2^+$ cells compared to the WT group (Figures 5C and 5D). These findings suggest that ISO stimulation or ADRB2 deficiency modulates bone mass through the coupling of angiogenesis and osteogenesis.

Pharmacological ADRB inhibition protected type H vessels and bone mass in estrogen deficiency

The obtained results prompted us to examine the pathological and therapeutic implications of sympathoadrenergic regulation of type H vessels. Our previous studies have shown an increase in the release of NE by sympathetic nerves in ovariectomized (OVX) mice,[39] indicating sympathetic nerve activation. Furthermore, mouse OVX replicates human estrogen deficiency which represents one major cause of bone loss often with psychological neural stress.[45,46] Therefore, we selected this model as a pathological condition of osteoporosis to investigate the regulatory role of sympathetic excitation on type H vessels. One week after the OVX procedure, immunofluorescence staining was performed to label TH^+ cells in the metaphysis in both the Sham and OVX groups to confirm the effects of OVX on the sympathetic nerves in mice. Images and quantitative analysis showed no significant changes in the density of TH^+ cells in the Sham and OVX groups one week after OVX modeling (Figures S8A and S8B). Nevertheless, by measuring the concentration of NE in the bone marrow of the Sham and OVX groups, we detected a significant increase in OVX mice compared to the Sham group, indicating an elevated level of sympathetic activation (Figure S8C). Collectively, these findings suggest that although the TH^+ sympathetic nerve does not alter in early OVX situations, sympathetic excitation occurs, which serves as a basis for pharmacological intervention.

Next, we accordingly administered PRO injections to OVX mice to inhibit potential ADRB activation under OVX conditions (Figure S2B). For mechanistic and target support, we found that the density of $NICD^+$ type H vessels was decreased in the OVX group compared to the Sham group, while after PRO treatment, the density of $NICD^+$ type H vessels was recovered (Figures 4E and 4F). Furthermore, $RUNX2^+$ cell staining and quantitative analysis demonstrated a significant decrease in the density of $RUNX2^+$ cells in the OVX group compared to the Sham group, whereas, after PRO treatment, an increase in the density of $RUNX2^+$ cells was observed (Figures 5E and 5F). These results suggested that ADRB inhibition by PRO counteracted the pathological effect of sympathetic activation after OVX, indicating that PRO may serve as an effective treatment for the decrease of type H vessels and bone mass under estrogen deficiency.

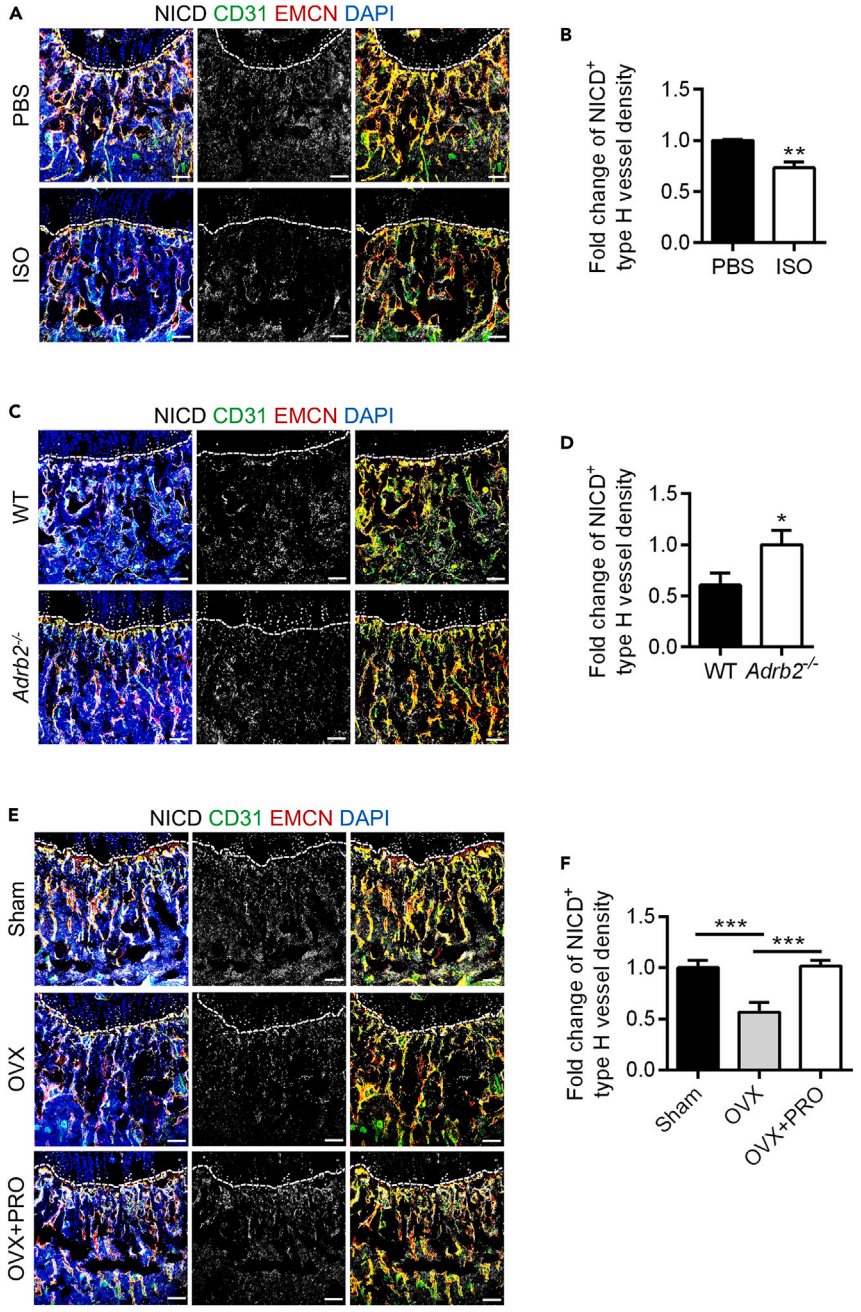

Figure 4. Notch signaling contributed to sympathoexcitation-regulated type H formation

(A) NICD (white), CD31 (green) and EMCN (red) co-immunostaining, counterstained by DAPI (blue), at metaphysis in femurs collected after daily intraperitoneal injections of ISO for one week. Dashed lines indicate the margin of growth plates. Scale bars, 100 μm.

(B) Quantification of NICD$^+$ type H vessel density (%) of (A). N = 3 per group.

(C) NICD (white), CD31 (green) and EMCN (red) co-immunostaining, counterstained by DAPI (blue), at metaphysis in femurs of WT and *Adrb2*$^{-/-}$ mice. Dashed lines indicate the margin of growth plates. Scale bars, 100 μm.

(D) Quantification of NICD$^+$ type H vessel density (%) of (C). N = 3 per group.

(E) NICD (white), CD31 (green) and EMCN (red) co-immunostaining, counterstained by DAPI (blue), at metaphysis in femurs collected after OVX and daily intraperitoneal injections of PRO for one week. Dashed lines indicate the margin of growth plates. Scale bars, 100 μm.

Figure 4. *Continued*

(F) Quantification of NICD$^+$ type H vessel density (%) of (E). $N = 3$ per group.

Data represent mean ± SD. Statistical analysis is performed by Student's *t* test for two-group comparison or by one-way analysis of variance followed by Newman–Keuls post-hoc tests for multiple comparisons. *, $p < 0.05$; **, $p < 0.01$; ***, $p < 0.001$.

To further validate the therapeutic effect of PRO treatment, *in vivo* examination of type H vessels and bone mass was conducted. The fluorescence images showed a decrease of type H vessel density in the OVX group compared to the Sham group and remarkable protection of type H vessels in the PRO group compared to the OVX group (Figure 6A), which was confirmed by further quantitative analysis (Figure 6B). Micro-CT analysis further showed that bone mass was significantly decreased in OVX group compared to Sham group and was maintained in the PRO group compared to OVX mice (Figure 6C), which was supported by the quantitative analysis of parameters of both trabecular and cortical bone (Figures 6D–6I). Taken together, the above results show that the pharmacological ADRB inhibition protected type H vessels and maintained bone mass under sympathetic activation in pathological circumstances.

DISCUSSION

The mammalian skeleton is a principal structural and endocrine organ that undergoes lifelong remodeling, which relies on niche microenvironments, including blood vessels and autonomic and sensory nerves.[21] Recent studies have identified type H vessels, a specialized vasculature subtype with distinct morphological and molecular properties and play a crucial role in formation and regeneration.[35,36] While the involvement of ADRBs in the SNS regulation of bone formation is well-established, their roles in angiogenesis and the significance of neurovascular crosstalk in the skeleton remain largely unknown.[22,47] In this study, we identified a close spatial association between sympathetic nerves and the type H endothelium, indicating a phenotypic connection. Furthermore, the negative effect on type H vessels exerted by sympathoexcitation was uncovered by ISO injection. Additionally, genetic ablation of ADRB2 was confirmed to maintain type H vessel density associated with preserved bone mass. Mechanistically, the indirect regulation of EC angiogenesis under sympathoexcitation through the paracrine effect of MSCs was unraveled *in vitro*. Moreover, the Notch signaling in ECs was revealed to underlie the sympathoexcitation-governed type H vessel formation, and corresponding effects on osteogenesis contributed to the regulation of bone mass. Importantly, the pharmacological ADRB inhibition promoted the formation of type H vessels and prevented bone loss in the OVX pathological condition. These findings highlight the marked phenotypic and functional relationship between sympathetic nerves and specialized vasculature in bone physiology and pathology. They also underscore the crucial implications of specific neurovascular coupling in bone homeostasis and regeneration.

Various physiological conditions, such as growth, aging, psychological stress and unloading, activate the SNS, which can disrupt the homeostasis and regeneration of various tissues.[39] Among the ADRs that respond to sympathoexcitation, ADRBs are thought to play a crucial role in mediating the effects of sympathetic outflow across the organism, particularly in relation to bone, which has become a focal point of research attention.[36] Moreover, it has been verified that bone development, remodeling and regeneration depend on microenvironmental factors,[48] among which vascular endothelium transports oxygen and nutrients as well as carries away waste products.[36] Specifically, type H vessels are located at the distal end of the bone arterial network, creating a metabolically active microenvironment that has privileged access to oxygen, nutrients, and growth factors released by ECs, maintaining perivascular osteoprogenitors, contributing to bone vasculature growth and coupling angiogenesis with osteogenesis, ultimately promoting the bone generation and regeneration.[35,36] Notably, the distribution of nerves and blood vessels in bone is intricately connected. However, whether sympathetic activation affects homeostasis and regeneration in bone through regulating specialized vasculature is still unknown. Our results show that in bone, the spatial distribution of the sympathetic nervous is closely related to type H vessels, suggesting the possibility of sympathetic control of type H vessel function for bone regulation and a new perspective for understanding the role and significance of specialized neurovascular coupling in bone.

To investigate the crosstalk effects of sympathetic nerves and type H vessels in bone homeostasis and regeneration, we conducted experiments using three different models that encompassed both physiological and pathological conditions. Notably, in the investigation of the impact of ADRB2 deficiency on type H vessels in mice, we observed a similar pattern as previously reported, where type H vessels in WT mice

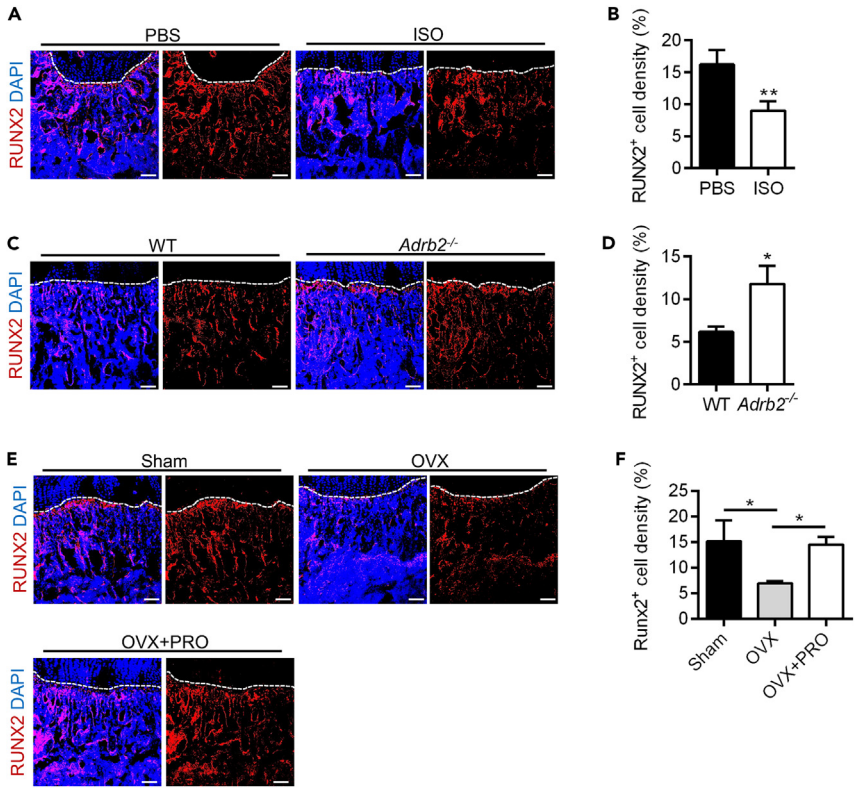

Figure 5. Sympathoexcitation regulated bone mass through the angiogenesis-osteogenesis coupling

(A and B) RUNX2 (red) immunostaining counterstained by DAPI (blue) and RUNX2$^+$ cell density (%) quantification at metaphysis in femurs collected after daily intraperitoneal injections of ISO for one week. Dashed lines indicate the margin of growth plates. Scale bars, 100 μm. $N = 3$ per group.

(C and D) RUNX2 (red) immunostaining counterstained by DAPI (blue) and RUNX2$^+$ cell density (%) quantification at metaphysis in femurs of 8 weeks WT and *Adrb2*$^{-/-}$ m$^{ice.}$ *Dashed lines indicate the margin of growth plates.* Scale bars, 100 μm. $N = 3$ per group.

(E and F) RUNX2 (red) immunostaining counterstained by DAPI (blue) and RUNX2$^+$ cell density (%) quantification at metaphysis in femurs collected after OVX and daily intraperitoneal injections of PRO for one week. Dashed lines indicate the margin of growth plates. Scale bars, 100 μm. $N = 3$ per group.

Data represent mean ± SD. Statistical analysis is performed by Student's *t* test for two-group comparison or by one-way analysis of variance followed by Newman–Keuls post-hoc tests for multiple comparisons. *, $p < 0.05$; **, $p < 0.01$.

decreased with age.[36,49] However, in the *Adrb2*$^{-/-}$ group, there was no significant age-related change in the density of type H vessels. The age-related decrease in type H vessels is a complex phenomenon influenced by various factors, including the coupling with osteogenesis,[36,49] environmental changes including oxidative stress[50] and hormone levels,[51] and intracellular signaling pathways, such as hypoxia-inducing factor-1 alpha (HIF-1α).[49] Besides, the increase in sympathetic activation with age also occurs, which might also be correlated with the decline of type H vessels. However, the impact of sympathetic nerve activation on type H vessels remains unclear. Therefore, the present findings of the sympathetic excitation effect on the maintenance of type H vessels in bone add to the current knowledge of regulatory mechanisms of type H vessels. It remains to be investigated whether ADRB2 deficiency influenced the age-related environmental and intracellular factors potentially contributing to the type H vessel alterations.

Additionally, in assessing bone mass, we found slight variations in cortical bone parameters among the different models. We propose two possible explanations for these findings. Firstly, Ct.Ar and Ct.Th represent different aspects of bone structure. Ct.Ar reflects the total area of bone tissue, while Ct.Th measures the thickness of bone tissue in a specific region. Thus, even within the same model, individual sample variations can contribute to differences in the trends of these two parameters. Secondly, based on our review of the relevant literature, we found that the sympatho-adrenergic influence on cortical

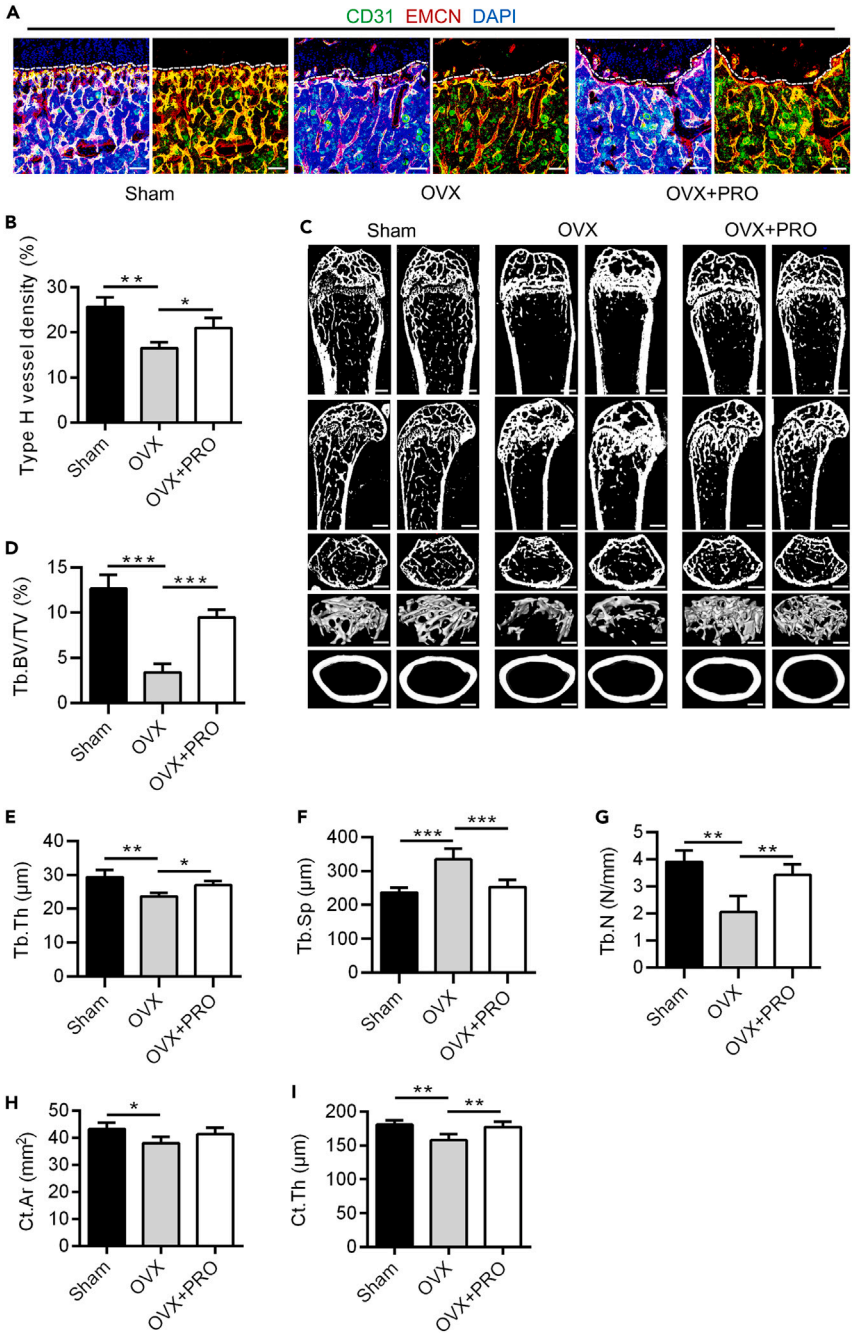

Figure 6. Pharmacological ADRB inhibition protected type H vessels and bone mass in estrogen deficiency

(A) CD31 (green) and EMCN (red) co-immunostaining, counterstained by DAPI (blue), at metaphysis of sham-operated mice, estrogen-deficient OVX mice and PRO-treated estrogen-deficient OVX mice after daily intraperitoneal injections of PRO for four weeks. Dashed lines indicate the margin of growth plates. Scale bar, 100 μm.

(B) Quantification of type H vessels density (%). *N* = 3 per group.

(C) Micro-CT analysis and 3D views of femurs of sham-operated mice, OVX mice and PRO-treated OVX mice. Scale bar of the lengthwise section, 500 μm. Scale bar of cross section and 3D views, 250 μm.

(D–G) Parameters analysis of trabecular bone mass. Tb.BV/TV, trabecular bone volume over tissue volume; Tb.Th, trabecular thickness; Tb.Sp, trabecular separation; Tb.N, trabecular number. *N* = 4 per group.

(H and I) Parameters analysis of cortical bone mass. Ct.Ar, cortical bone area; Ct.Th, cortical bone thickness. *N* = 4 per group.

Figure 6. *Continued*
Data represent mean ± SD. Statistical analysis is performed by Student's *t* test for two-group comparison or by one-way analysis of variance followed by Newman–Keuls post-hoc tests for multiple comparisons. *, $p < 0.05$; **, $p < 0.01$; ***, $p < 0.001$.

bone becomes more prominent as the mice age. For example, Bouxsein et al. demonstrated that 16-week-old β-less mice exhibited a more prominent maintenance effect on Ct.Th compared to 6-week-old β-less mice. In this study, we employed 8-week-old and 12-week-old mice for micro-CT assessments, and it is possible that age-related factors contributed to the less prominent changes in cortical values, as well as in the 4-week-old mouse counterparts. Overall, all these findings significantly contribute to our understanding of the complex interplay between the SNS and the specialized vasculature in regulating bone homeostasis and regeneration. Considering that sympathoexcitation often occurs under stress conditions and that psychological stress may lead to bone loss, whether the sympathetic nerve-type H vessel coupling serves as a mechanism underlying stress-induced osteopenia will be interesting to investigate in the future.

In bone homeostasis and the process of regeneration, angiogenesis plays a crucial role in regulating the maintenance and formation of blood vessels, which involves providing essential nutrients and signaling support to cells, promoting tissue structure and functional restoration.[35,51] The involvement of the Notch pathway in regulating the formation and maintenance of type H vessels has been established.[44] However, it remains unclear whether the Notch pathway is also involved in the regulation of type H vessels under sympathoexcitation. In this study, our results demonstrated responsive changes in the expression of NICD, a key active component of the Notch pathway, under three different types of sympathetic regulation models. This provides the first evidence of the involvement of the Notch pathway in the regulation of type H vessels by sympathetic activation.

Moreover, angiogenesis in tissue regeneration is regulated through both cell-autonomous and non-autonomous mechanisms. The cell-autonomous regulation is achieved through angiogenic response and EC metabolic adaption,[52] while the non-autonomous regulation is mediated through the indirect effects of vascular pericytes, including MSCs.[53,54] While sympathetic innervation has been reported to regulate MSC function, primarily in terms of proliferation and differentiation rather than endothelial function such as angiogenesis,[55] the extent to which MSCs participate in the angiogenic process under sympathetic activity remains unknown. Our results confirmed the expression of ADRB1/2/3 in both human and mouse MSCs and ECs, and that MSCs indirectly regulate EC angiogenesis under sympathoexcitation through paracrine effects. Notably, we used human cells as the cell source for rapid and convenient analysis of the responses of MSCs and ECs to sympathetic regulation and provide clinical relevance, as also seen in published papers.[56,57] Although this conclusion has yet to be validated *in vivo*, our findings open up a new direction for further investigations into the effects of sympathetic activation on the density and function of type H vessels. Besides, although we have discovered the involvement of paracrine factors in the angiogenesis process of sympathetic nerve activation, the specific regulatory components are yet to be fully elucidated. In recent years, there have been increasing studies on extracellular vesicles (EVs) as intercellular communication.[58] Exploring whether and how EVs play a role in this regulation is a promising area for future research.

Intriguingly, ADRBs have emerged as potential targets for mitigating bone loss in multiple osteopenic disorders.[59,60] Particularly, pathological conditions, such as estrogen deficiency, lead to sympathetic activation and osteopenia.[48] The regulation of the sympathetic nerves on bone mass presents a promising target for osteoporosis treatment.[39,48] Previous studies, including our own, have demonstrated that the concentration of NE, the neurotransmitter of sympathetic nerve fibers, increases in the serum of OVX mice and that genetic or pharmacological inhibition of ADRB2 can alleviate the bone loss resulting from estrogen deficiency or unloading.[39,61] However, the specific role of type H vessel recovery in ADRB intervention to counteract sympathoexcitation-induced osteopenia remains unclear. Notably, in the context of the known impact of castration-mediated sex hormone deficiency, it has a similar impact on osteoporosis development and treatment regardless of sex,[62] and we ultimately chose the OVX model to better mimic clinical relevance. Our findings indicated that pharmacological ADRB inhibition leads to a significant increase of type H vessels in OVX mice, along with restored bone mass, providing a new mechanism underlying ADRB antagonist-induced osteopenia alleviation and further supporting the establishment of vascular-targeted anabolic therapy for postmenopausal osteoporosis.

In conclusion, our study has revealed the specialized spatial and functional neurovascular crosstalk, demonstrating that ADRBs, particularly ADRB2, negatively regulate type H vasculature and bone homeostasis. Our results also provide insights into the regulatory mechanism of sympathoexcitation control of angiogenesis, and importantly, ADRB inhibition protects against bone loss induced by estrogen deficiency through type H vessel recovery. These findings uncover a specific form of neurovascular coupling and indicate a neural signaling-based and vasculature-targeted approach for osteoanabolic therapies.

Limitations of the study

When considering these results, it should be noticed that there are certain limitations regarding the sex-specific selection in the three models in this study. However, the selection of the OVX model, which is more often used as an established model for osteoporotic research compared to orchidectomy (ORX), was aimed at better representing the clinical condition of postmenopausal osteoporosis. Additionally, in the ISO and ADRB2-deficient models, male mice were included with relatively stable hormone levels to minimize the potentially interfering factor of hormonal fluctuations present in female animals, which enabled us to explore the relationship between sympathetic cues and type H vessels conveniently.

STAR★METHODS

Detailed methods are provided in the online version of this paper and include the following:

- KEY RESOURCES TABLE
- RESOURCE AVAILABILITY
  - Lead contact
  - Materials availability
  - Data and code availability
- EXPERIMENTAL MODEL AND PARTICIPANT DETAILS
  - Experimental model
  - Participant details
- QUANTIFICATION AND STATISTICAL ANALYSIS

SUPPLEMENTAL INFORMATION

Supplemental information can be found online at https://doi.org/10.1016/j.isci.2023.107455.

ACKNOWLEDGMENTS

This work is supported by grants from the National Natural Science Foundation of China (81930025 to B.D.S., 32000974 to B.D.S., 82071136 to Y.J.C., 82201090 to Y.J.Z.), the Independent Project of State Key Laboratory of Military Stomatology (2019ZA02 to Y.J.C.) and the Special project of National Clinical Research Center for Oral Diseases (LCB202006 to L.K.).

AUTHOR CONTRIBUTIONS

Conceptualization, B.D.S., Y.J.C., and L.K.; Methodology, H.K.X., J.X.L., and C.X.Z.; Software, S.J.X. and C.H.H.; Validation, Q.L.; Formal analysis, H.K.X., J.X.L., and C.X.Z.; Investigation, H.K.X., J.X.L., and C.X.Z.; Resources, Y.J.Z.; Data curation, L.L., C.M., J.Y.T., Y.Y., and Y.C.; Writing—original draft preparation, H.K.X., J.X.L., and C.X.Z.; Writing—review and editing, S.J.X., C.H.H., L.L., C.M., J.Y.T., Y.Y., Y.C., Q.L., Y.J.Z., B.D.S., Y.J.C., and L.K.; Visualization, H.K.X., J.X.L., and C.X.Z.; Supervision, B.D.S., Y.J.C., and L.K.; Project administration, B.D.S., Y.J.C., and L.K.; Funding acquisition, B.D.S., Y.J.C., L.K., and Y.J.Z. All authors have read and agreed to the published version of the manuscript.

DECLARATION OF INTERESTS

The authors declare no conflict of interest.

Received: March 15, 2023
Revised: June 13, 2023
Accepted: July 19, 2023
Published: July 22, 2023

REFERENCES

1. Distler, A., Liebau, H., and Wolff, H.P. (1965). Action of angiotensin on sympathetic nerve endings in isolated blood vessels. Nature *207*, 764–765. https://doi.org/10.1038/207764a0.

2. Makita, T. (2013). Nerve control of blood vessel patterning. Dev. Cell *24*, 340–341. https://doi.org/10.1016/j.devcel.2013.02.003.

3. Kovach, A.G., and Takacs, L. (1953). Response of the vascular system to sympathetic stimuli during shock. Nature *171*, 433–434. https://doi.org/10.1038/171433a0.

4. Schaeffer, S., and Iadecola, C. (2021). Revisiting the neurovascular unit. Nat. Neurosci. *24*, 1198–1209. https://doi.org/10.1038/s41593-021-00904-7.

5. Mastorakos, P., and McGavern, D. (2019). The anatomy and immunology of vasculature in the central nervous system. Sci. Immunol. *4*, eaav0492. https://doi.org/10.1126/sciimmunol.aav0492.

6. Aalkjær, C., Nilsson, H., and De Mey, J.G.R. (2021). Sympathetic and Sensory-Motor Nerves in Peripheral Small Arteries. Physiol. Rev. *101*, 495–544. https://doi.org/10.1152/physrev.00007.2020.

7. Armstrong, J.M., Blackwell, G.J., Flower, R.J., McGiff, J.C., Mullane, K.M., and Vane, J.R. (1976). Genetic hypertension in rats is accompanied by a defect in renal prostaglandin catabolism. Nature *260*, 582–586. https://doi.org/10.1038/260582a0.

8. Tarazi, R.C. (1974). Sympathomimetic agents in the treatment of shock. Ann. Intern. Med. *81*, 364–371. https://doi.org/10.7326/0003-4819-81-3-364.

9. Sims, S.M., Singer, J.J., and Walsh, J.V., Jr. (1988). Antagonistic adrenergic-muscarinic regulation of M current in smooth muscle cells. Science *239*, 190–193. https://doi.org/10.1126/science.2827305.

10. Scheid, C.R., Honeyman, T.W., and Fay, F.S. (1979). Mechanism of beta-adrenergic relaxation of smooth muscle. Nature *277*, 32–36. https://doi.org/10.1038/277032a0.

11. Cocks, T.M., and Angus, J.A. (1983). Endothelium-dependent relaxation of coronary arteries by noradrenaline and serotonin. Nature *305*, 627–630. https://doi.org/10.1038/305627a0.

12. Vandecasteele, G., Eschenhagen, T., Scholz, H., Stein, B., Verde, I., and Fischmeister, R. (1999). Muscarinic and beta-adrenergic regulation of heart rate, force of contraction and calcium current is preserved in mice lacking endothelial nitric oxide synthase. Nat. Med. *5*, 331–334. https://doi.org/10.1038/6553.

13. Tymko, M.M., Lawley, J.S., Ainslie, P.N., Hansen, A.B., Hofstaetter, F., Rainer, S., Amin, S., Moralez, G., Gasho, C., Vizcardo-Galindo, G., et al. (2020). Global Reach 2018 Heightened alpha-Adrenergic Signaling Impairs Endothelial Function During Chronic Exposure to Hypobaric Hypoxia. Circ. Res. *127*, e1–e13. https://doi.org/10.1161/CIRCRESAHA.119.316053.

14. Swenson, E.R. (2020). Sympathetic Nervous System Activation and Vascular Endothelial Function With Chronic Hypoxia. Circ. Res. *127*, 247–248. https://doi.org/10.1161/CIRCRESAHA.120.317114.

15. Ungvari, Z., Tarantini, S., Kiss, T., Wren, J.D., Giles, C.B., Griffin, C.T., Murfee, W.L., Pacher, P., and Csiszar, A. (2018). Endothelial dysfunction and angiogenesis impairment in the ageing vasculature. Nat. Rev. Cardiol. *15*, 555–565. https://doi.org/10.1038/s41569-018-0030-z.

16. Chen, H.I., Li, H.T., and Chen, C.C. (1994). Physical conditioning decreases norepinephrine-induced vasoconstriction in rabbits. Possible roles of norepinephrine-evoked endothelium-derived relaxing factor. Circulation *90*, 970–975. https://doi.org/10.1161/01.cir.90.2.970.

17. Massion, P.B., Dessy, C., Desjardins, F., Pelat, M., Havaux, X., Belge, C., Moulin, P., Guiot, Y., Feron, O., Janssens, S., and Balligand, J.L. (2004). Cardiomyocyte-restricted overexpression of endothelial nitric oxide synthase (NOS3) attenuates beta-adrenergic stimulation and reinforces vagal inhibition of cardiac contraction. Circulation *110*, 2666–2672. https://doi.org/10.1161/01.CIR.0000145608.80855.BC.

18. Fukuchi, M., Hussain, S.N., and Giaid, A. (1998). Heterogeneous expression and activity of endothelial and inducible nitric oxide synthases in end-stage human heart failure: their relation to lesion site and beta-adrenergic receptor therapy. Circulation *98*, 132–139. https://doi.org/10.1161/01.cir.98.2.132.

19. Galasso, G., De Rosa, R., Ciccarelli, M., Sorriento, D., Del Giudice, C., Strisciuglio, T., De Biase, C., Luciano, R., Piccolo, R., Pierri, A., et al. (2013). beta2-Adrenergic receptor stimulation improves endothelial progenitor cell-mediated ischemic neoangiogenesis. Circ. Res. *112*, 1026–1034. https://doi.org/10.1161/CIRCRESAHA.111.300152.

20. Lee, S.J., Kim, D.Y., Yun, J., Choi, S.H., Jung, S.Y., Kang, S., Park, J.H., Kim, Y.J., Ha, J.S., Ji, S.T., et al. (2018). Angiotensin II Attenuates the Bioactivities of Human Endothelial Progenitor Cells via Downregulation of beta2-Adrenergic Receptor. Stem Cells Int. *2018*, 7453161. https://doi.org/10.1155/2018/7453161.

21. Qin, Q., Lee, S., Patel, N., Walden, K., Gomez-Salazar, M., Levi, B., and James, A.W. (2022). Neurovascular coupling in bone regeneration. Exp. Mol. Med. *54*, 1844–1849. https://doi.org/10.1038/s12276-022-00899-6.

22. Elefteriou, F. (2018). Impact of the Autonomic Nervous System on the Skeleton. Physiol. Rev. *98*, 1083–1112. https://doi.org/10.1152/physrev.00014.2017.

23. Elefteriou, F., Ahn, J.D., Takeda, S., Starbuck, M., Yang, X., Liu, X., Kondo, H., Richards, W.G., Bannon, T.W., Noda, M., et al. (2005). Leptin regulation of bone resorption by the sympathetic nervous system and CART. Nature *434*, 514–520. https://doi.org/10.1038/nature03398.

24. Fu, L., Patel, M.S., Bradley, A., Wagner, E.F., and Karsenty, G. (2005). The molecular clock mediates leptin-regulated bone formation. Cell *122*, 803–815. https://doi.org/10.1016/j.cell.2005.06.028.

25. Ducy, P., Amling, M., Takeda, S., Priemel, M., Schilling, A.F., Beil, F.T., Shen, J., Vinson, C., Rueger, J.M., and Karsenty, G. (2000). Leptin inhibits bone formation through a hypothalamic relay: a central control of bone mass. Cell *100*, 197–207. https://doi.org/10.1016/s0092-8674(00)81558-5.

26. Takeda, S., Elefteriou, F., Levasseur, R., Liu, X., Zhao, L., Parker, K.L., Armstrong, D., Ducy, P., and Karsenty, G. (2002). Leptin regulates bone formation via the sympathetic nervous system. Cell *111*, 305–317. https://doi.org/10.1016/s0092-8674(02)01049-8.

27. Pierroz, D.D., Bonnet, N., Bianchi, E.N., Bouxsein, M.L., Baldock, P.A., Rizzoli, R., and Ferrari, S.L. (2012). Deletion of beta-adrenergic receptor 1, 2, or both leads to different bone phenotypes and response to mechanical stimulation. J. Bone Miner. Res. *27*, 1252–1262. https://doi.org/10.1002/jbmr.1594.

28. Bouxsein, M.L., Devlin, M.J., Glatt, V., Dhillon, H., Pierroz, D.D., and Ferrari, S.L. (2009). Mice lacking beta-adrenergic receptors have increased bone mass but are not protected from deleterious skeletal effects of ovariectomy. Endocrinology *150*, 144–152. https://doi.org/10.1210/en.2008-0843.

29. Khosla, S., Drake, M.T., Volkman, T.L., Thicke, B.S., Achenbach, S.J., Atkinson, E.J., Joyner, M.J., Rosen, C.J., Monroe, D.G., and Farr, J.N. (2018). Sympathetic beta1-adrenergic signaling contributes to regulation of human bone metabolism. J. Clin. Invest. *128*, 4832–4842. https://doi.org/10.1172/JCI122151.

30. Maryanovich, M., Zahalka, A.H., Pierce, H., Pinho, S., Nakahara, F., Asada, N., Wei, Q., Wang, X., Ciero, P., Xu, J., et al. (2018). Adrenergic nerve degeneration in bone marrow drives aging of the hematopoietic stem cell niche. Nat. Med. *24*, 782–791. https://doi.org/10.1038/s41591-018-0030-x.

31. Ferraro, F., Lymperi, S., Méndez-Ferrer, S., Saez, B., Spencer, J.A., Yeap, B.Y., Masselli, E., Graiani, G., Prezioso, L., Rizzini, E.L., et al. (2011). Diabetes impairs hematopoietic stem cell mobilization by altering niche function. Sci. Transl. Med. *3*, 104ra101. https://doi.org/10.1126/scitranslmed.3002191.

32. Arranz, L., Sánchez-Aguilera, A., Martín-Pérez, D., Isern, J., Langa, X., Tzankov, A., Lundberg, P., Muntión, S., Tzeng, Y.S., Lai, D.M., et al. (2014). Neuropathy of haematopoietic stem cell niche is essential for myeloproliferative neoplasms. Nature *512*, 78–81. https://doi.org/10.1038/nature13383.

33. Zhu, S., Bennett, S., Kuek, V., Xiang, C., Xu, H., Rosen, V., and Xu, J. (2020). Endothelial cells produce angiocrine factors to regulate bone and cartilage via versatile mechanisms. Theranostics *10*, 5957–5965. https://doi.org/10.7150/thno.45422.

34. Kalucka, J., de Rooij, L.P.M.H., Goveia, J., Rohlenova, K., Dumas, S.J., Meta, E., Conchinha, N.V., Taverna, F., Teuwen, L.A., Veys, K., et al. (2020). Single-Cell Transcriptome Atlas of Murine Endothelial Cells. Cell *180*, 764–779.e20. https://doi.org/10.1016/j.cell.2020.01.015.

35. Peng, Y., Wu, S., Li, Y., and Crane, J.L. (2020). Type H blood vessels in bone modeling and remodeling. Theranostics *10*, 426–436. https://doi.org/10.7150/thno.34126.

36. Kusumbe, A.P., Ramasamy, S.K., and Adams, R.H. (2014). Coupling of angiogenesis and osteogenesis by a specific vessel subtype in bone. Nature *507*, 323–328. https://doi.org/10.1038/nature13145.

37. Wee, N.K.Y., Lorenz, M.R., Bekirov, Y., Jacquin, M.F., and Scheller, E.L. (2019). Shared Autonomic Pathways Connect Bone Marrow and Peripheral Adipose Tissues Across the Central Neuraxis. Front. Endocrinol. *10*, 668. https://doi.org/10.3389/fendo.2019.00668.

38. Wang, Q., Liu, K., Yang, L., Wang, H., and Yang, J. (2019). BoneClear: whole-tissue immunolabeling of the intact mouse bones for 3D imaging of neural anatomy and pathology. Cell Res. *29*, 870–872. https://doi.org/10.1038/s41422-019-0217-9.

39. Hu, C.H., Sui, B.D., Liu, J., Dang, L., Chen, J., Zheng, C.X., Shi, S., Zhao, N., Dang, M.Y., He, X.N., et al. (2022). Sympathetic Neurostress Drives Osteoblastic Exosomal MiR-21 Transfer to Disrupt Bone Homeostasis and Promote Osteopenia. Small Methods *6*, e2100763. https://doi.org/10.1002/smtd.202100763.

40. Schwab, K.E., and Gargett, C.E. (2007). Co-expression of two perivascular cell markers isolates mesenchymal stem-like cells from human endometrium. Hum. Reprod. *22*, 2903–2911. https://doi.org/10.1093/humrep/dem265.

41. Yianni, V., and Sharpe, P.T. (2019). Perivascular-Derived Mesenchymal Stem Cells. J. Dent. Res. *98*, 1066–1072. https://doi.org/10.1177/0022034519862258.

42. Radmanesh, F., Sadeghi Abandansari, H., Ghanian, M.H., Pahlavan, S., Varzideh, F., Yakhkeshi, S., Alikhani, M., Moradi, S., Braun, T., and Baharvand, H. (2021). Hydrogel-mediated delivery of microRNA-92a inhibitor polyplex nanoparticles induces localized angiogenesis. Angiogenesis *24*, 657–676. https://doi.org/10.1007/s10456-021-09778-6.

43. Wang, Y., Dong, L., Zhong, H., Yang, L., Li, Q., Su, C., Gu, W., and Qian, Y. (2019). Extracellular Vesicles (EVs) from Lung Adenocarcinoma Cells Promote Human Umbilical Vein Endothelial Cell (HUVEC) Angiogenesis through Yes Kinase-associated Protein (YAP) Transport. Int. J. Biol. Sci. *15*, 2110–2118. https://doi.org/10.7150/ijbs.31605.

44. Liu, L., Zheng, C.X., Zhao, N., Zhu, T., Hu, C.B., Zhang, N., Chen, J., Zhang, K.C., Zhang, S., Liu, J.X., et al. (2023). Mesenchymal Stem Cell Aggregation-Released Extracellular Vesicles Induce CD31(+) EMCN(+) Vessels in Skin Regeneration and Improve Diabetic Wound Healing. Adv. Healthc. Mater.e2300019 https://doi.org/10.1002/adhm.202300019.

45. Deng, Y.X., He, W.G., Cai, H.J., Jiang, J.H., Yang, Y.Y., Dan, Y.R., Luo, H.H., Du, Y., Chen, L., and He, B.C. (2021). Analysis and Validation of Hub Genes in Blood Monocytes of Postmenopausal Osteoporosis Patients. Front. Endocrinol. *12*, 815245. https://doi.org/10.3389/fendo.2021.815245.

46. Jia, X., Jia, L., Mo, L., Yuan, S., Zheng, X., He, J., Chen, V., Guo, Q., Zheng, L., Yuan, Q., et al. (2019). Berberine Ameliorates Periodontal Bone Loss by Regulating Gut Microbiota. J. Dent. Res. *98*, 107–116. https://doi.org/10.1177/0022034518797275.

47. Zaidi, M. (2005). Neural surveillance of skeletal homeostasis. Cell Metab. *1*, 219–221. https://doi.org/10.1016/j.cmet.2005.03.006.

48. Sui, B., Liu, J., Zheng, C., Dang, L., Chen, J., Cao, Y., Zhang, K., Liu, L., Dang, M., Zhang, L., et al. (2022). Targeted inhibition of osteoclastogenesis reveals the pathogenesis and therapeutics of bone loss under sympathetic neurostress. Int. J. Oral Sci. *14*, 39. https://doi.org/10.1038/s41368-022-00193-1.

49. Chen, J., Li, M., Liu, A.Q., Zheng, C.X., Bao, L.H., Chen, K., Xu, X.L., Guan, J.T., Bai, M., Zhou, T., et al. (2020). Gli1(+) Cells Couple with Type H Vessels and Are Required for Type H Vessel Formation. Stem Cell Rep. *15*, 110–124. https://doi.org/10.1016/j.stemcr.2020.06.007.

50. Hu, X.F., Xiang, G., Wang, T.J., Ma, Y.B., Zhang, Y., Yan, Y.B., Zhao, X., Wu, Z.X., Feng, Y.F., and Lei, W. (2021). Impairment of type H vessels by NOX2-mediated endothelial oxidative stress: critical mechanisms and therapeutic targets for bone fragility in streptozotocin-induced type 1 diabetic mice. Theranostics *11*, 3796–3812. https://doi.org/10.7150/thno.50907.

51. Huang, J., Yin, H., Rao, S.S., Xie, P.L., Cao, X., Rao, T., Liu, S.Y., Wang, Z.X., Cao, J., Hu, Y., et al. (2018). Harmine enhances type H vessel formation and prevents bone loss in ovariectomized mice. Theranostics *8*, 2435–2446. https://doi.org/10.7150/thno.22144.

52. Adams, R.H., and Alitalo, K. (2007). Molecular regulation of angiogenesis and lymphangiogenesis. Nat. Rev. Mol. Cell Biol. *8*, 464–478. https://doi.org/10.1038/nrm2183.

53. Guiducci, S., Manetti, M., Romano, E., Mazzanti, B., Ceccarelli, C., Dal Pozzo, S., Milia, A.F., Bellando-Randone, S., Fiori, G., Conforti, M.L., et al. (2011). Bone marrow-derived mesenchymal stem cells from early diffuse systemic sclerosis exhibit a paracrine machinery and stimulate angiogenesis in vitro. Ann. Rheum. Dis. *70*, 2011–2021. https://doi.org/10.1136/ard.2011.150607.

54. Zhang, L., Jiao, G., Ren, S., Zhang, X., Li, C., Wu, W., Wang, H., Liu, H., Zhou, H., and Chen, Y. (2020). Exosomes from bone marrow mesenchymal stem cells enhance fracture healing through the promotion of osteogenesis and angiogenesis in a rat model of nonunion. Stem Cell Res. Ther. *11*, 38. https://doi.org/10.1186/s13287-020-1562-9.

55. Hu, B., Lv, X., Chen, H., Xue, P., Gao, B., Wang, X., Zhen, G., Crane, J.L., Pan, D., Liu, S., et al. (2020). Sensory nerves regulate mesenchymal stromal cell lineage commitment by tuning sympathetic tones. J. Clin. Invest. *130*, 3483–3498. https://doi.org/10.1172/JCI131554.

56. Pérez Piñero, C., Bruzzone, A., Sarappa, M.G., Castillo, L.F., and Lüthy, I.A. (2012). Involvement of alpha2- and beta2-adrenoceptors on breast cancer cell proliferation and tumour growth regulation. Br. J. Pharmacol. *166*, 721–736. https://doi.org/10.1111/j.1476-5381.2011.01791.x.

57. Tuvia, S., Moses, A., Gulayev, N., Levin, S., and Korenstein, R. (1999). Beta-adrenergic agonists regulate cell membrane fluctuations of human erythrocytes. J. Physiol. *516*, 781–792. https://doi.org/10.1111/j.1469-7793.1999.0781u.x.

58. Zheng, C., Sui, B., Zhang, X., Hu, J., Chen, J., Liu, J., Wu, D., Ye, Q., Xiang, L., Qiu, X., et al. (2021). Apoptotic vesicles restore liver macrophage homeostasis to counteract type 2 diabetes. J. Extracell. Vesicles *10*, e12109. https://doi.org/10.1002/jev2.12109.

59. Baek, K., and Bloomfield, S.A. (2009). Beta-adrenergic blockade and leptin replacement effectively mitigate disuse bone loss. J. Bone Miner. Res. *24*, 792–799. https://doi.org/10.1359/jbmr.081241.

60. Hanyu, R., Wehbi, V.L., Hayata, T., Moriya, S., Feinstein, T.N., Ezura, Y., Nagao, M., Saita, Y., Hemmi, H., Notomi, T., et al. (2012). Anabolic action of parathyroid hormone regulated by the beta2-adrenergic receptor. Proc. Natl. Acad. Sci. USA *109*, 7433–7438. https://doi.org/10.1073/pnas.1109036109.

61. He, J.Y., Jiang, L.S., and Dai, L.Y. (2011). The roles of the sympathetic nervous system in osteoporotic diseases: A review of experimental and clinical studies. Ageing Res. Rev. *10*, 253–263. https://doi.org/10.1016/j.arr.2011.01.002.

62. Sui, B.D., Chen, J., Zhang, X.Y., He, T., Zhao, P., Zheng, C.X., Li, M., Hu, C.H., and Jin, Y. (2018). Gender-independent efficacy of mesenchymal stem cell therapy in sex hormone-deficient bone loss via immunosuppression and resident stem cell recovery. Exp. Mol. Med. *50*, 1–14. https://doi.org/10.1038/s12276-018-0192-0.

63. Sui, B.D., Hu, C.H., Zheng, C.X., Shuai, Y., He, X.N., Gao, P.P., Zhao, P., Li, M., Zhang, X.Y., He, T., et al. (2017). Recipient Glycemic Microenvironments Govern Therapeutic Effects of Mesenchymal Stem Cell Infusion on Osteopenia. Theranostics *7*, 1225–1244. https://doi.org/10.7150/thno.18181.

64. Bouxsein, M.L., Boyd, S.K., Christiansen, B.A., Guldberg, R.E., Jepsen, K.J., and Müller, R. (2010). Guidelines for assessment of bone microstructure in rodents using micro-computed tomography. J. Bone Miner. Res. *25*, 1468–1486. https://doi.org/10.1002/jbmr.141.

65. Zheng, C.X., Chen, J., Tian, J.Y., Huang, X.Y., Jin, Y., and Sui, B.D. (2022). Optimized immunofluorescence staining protocol for identifying resident mesenchymal stem cells in bone using LacZ transgenic mice. STAR Protoc. *3*, 101674. https://doi.org/10.1016/j.xpro.2022.101674.

66. Xing, S.J., Zhang, K.C., Tang, S.Y., Liu, L., Cao, Y., Zheng, C.X., Sui, B.D., and Jin, Y. (2022). Isolation, Characterization, and Therapeutic Application of Extracellular Vesicles from Cultured Human Mesenchymal Stem Cells. J. Vis. Exp. https://doi.org/10.3791/64135.

STAR★METHODS

KEY RESOURCES TABLE

REAGENT or RESOURCE	SOURCE	IDENTIFIER
Antibodies		
Mouse/Rat CD31/PECAM-1 Alexa Fluor® 488-conjugated Antibody	R&D Systems	Cat# FAB3628G; RRID: AB_10972784
Endomucin (V.7C7) antibody	Santa Cruz Biotechnology	Cat# sc-65495; RRID: AB_2100037
Anti-Tyrosine Hydroxylase Antibody	Millipore	Cat# ab152; RRID: AB_390204
Cy3-AffiniPure Goat Anti-Rat IgG(H + L)	Yeasen	Cat# 33308ES60
Goat Anti-Rabbit IgG H&L (Cy5 ®) preadsorbed ab6564	Abcam	Cat# ab6564; RRID: AB_955061
β1-Adrenergic Receptor Rabbit pAb	ABclonal	Cat# A20818
ADRB1 Polyclonal antibody	Proteintech	Cat# 28323-1-AP
ADRB2 Rabbit pAb	ABclonal	Cat# A2048
ADRB2 Polyclonal antibody	Proteintech	Cat# 29864
ADRB3 Rabbit pAb	ABclonal	Cat# A8607
GAPDH(Clone:1A6), Mouse mAb	Yeasen	Cat# 30201ES20
β-actin, Mouse mAb	Yeasen	Cat# 30101ES60
Notch1 (D1E11) XP® Rabbit mAb	Cell Signaling Technology	Cat# 3608S
RUNX2 (F-2) antibody	Santa Cruz Biotechnology	Cat# sc-390351; RRID: AB_2892645
Chemicals, peptides, and recombinant proteins		
Isoprenaline hydrochloride	MedChemExpress	Cat# HY-B0468
Propranolol	MedChemExpress	Cat# HY-B0573B
4% polyformaldehyde (PFA)	Sigma	Cat# 1004965000
17% Ethylene Diamine Tetraacetic Acid (EDTA) decalcification solution	Proandy	Cat# 10218-1
Optimal cutting temperature (OCT) compound	Leica	Cat# 3801480
0.3% Triton X-100	Sigma	Cat# X100PC-5ML
Goat serum	BOSTER	Cat# AR0009
L-glutamine	Invitrogen	Cat# 35050061
Penicillin/streptomycin	Invitrogen	Cat# 15070063
Matrigel	Shanghai Nova Medical Technology	Cat# 0827775
Mounting Medium With DAPI-aqueous fluoroshield	Abcam	Cat# ab104139
Cell Lysis Buffer	Beyotime	Cat# P0013J
Protease inhibitor	Roche	Cat# P8215
5% Bovine Serum Albumin (BSA)	MP Biomedicals	Cat# 0881066-CF
Tris-buffered saline-Tween (TBS-T)	Solarbio	Cat# T1081-10
Trizol Reagent	Takara	Cat# T9424
α-MEM	Invitrogen	Cat# 12571-048
Fetal bovine serum (FBS)	Sijiqing	Cat# 11011-8611

(*Continued on next page*)

Continued

REAGENT or RESOURCE	SOURCE	IDENTIFIER
Endothelial cell medium (ECM)	Sciencell	Cat# 1001
Critical commercial assays		
BCA Protein Assay Kit	TIANGEN	Cat# PA115-02
Polyvinylidene fluoride membranes	Roche	Cat# GVWP02500
Chemiluminescence kit	4A Biotech	Cat# 4AW011-100
Abnova™ Epinephrine/Norepinephrine ELISA Kit	Abnova	Cat# KA1877
SYBR Premx Ex Taq II Kit	Takara	Cat# S5193
Experimental models: Cell lines		
HUVEC	ATCC	Cat# CRL-1730; RRID: CVCL_2959
MUVEC	Otwo Biotech	Cat# HTX3109
Experimental models: Organisms/strains		
Mouse: C57BL/6J	The Laboratory Animal Center of the Fourth Military Medical University	N/A
Mouse: FVB.129-*Adrb2*^{tm1Bkk}/J	The Jackson Laboratory	Cat#JAX: 031496; RRID: IMSR_JAX:031496
Oligonucleotides		
qRT-PCR primers	Sangon	N/A
Software and algorithms		
GraphPad Prism	GraphPad	RRID: SCR_002798
ImageJ 1.47	National Institute of Health	RRID: SCR_003070
GE Volume Viewer	GE Healthcare	RRID: SCR_023417
VGStudio MAX software	Volume Graphocs	RRID: SCR_017997
FV10-ASW Viewer software	Olympus	RRID: SCR_014215
Gel imaging system	Tanon	N/A
Real-Time System	Bio-Rad	RRID: SCR_018057
CFX Manager software	Bio-Rad	RRID: SCR_017251

RESOURCE AVAILABILITY

Lead contact

Further information and requests for resources and reagents should be directed to and will be fulfilled by the lead contact, Bing-Dong Sui (bingdong@fmmu.edu.cn).

Materials availability

All unique/stable reagents generated in this study are available from the lead contact with a completed materials transfer agreement.

Data and code availability

- All data reported in this paper will be shared by the lead contact upon request.
- This paper does not report original code.
- Any additional information required to reanalyze the data reported in this work is available from the lead contact upon request.

EXPERIMENTAL MODEL AND PARTICIPANT DETAILS

Experimental model

All animal experiments were performed in compliance with the relevant laws and ethical regulations, following the Guidelines of Intramural Animal Use and Care Committees of Fourth Military Medical University, approved by the Ethics Committee of Fourth Military Medical University (Protocol No. 2014-073), and following the ARRIVE guidelines. Male and female C57BL/6 mice at 8 weeks of age, which we have used in previous studies, were purchased from the Laboratory Animal Center of the Fourth Military Medical University.[48] Male WT and *Adrb2*$^{-/-}$ mice at the same ages (4/8/12 w) were obtained from the Jackson Laboratory. All mice were maintained under specific pathogen-free conditions with a temperature of 24°C, 12-h light/dark cycles and 50% humidity, and were given *ad libitum* access to food and water.

Participant details

In vivo experiments

To induce an ovariectomy (OVX) model, 8-week-old female mice underwent a bilateral OVX by the dorsal approach under general anesthesia and were modeled for 1 month (40). The ISO (MedChemExpress, USA) was dissolved in PBS as 1 mg/mL, stored at −20°C, and intraperitoneally injected at a dose of 10 mg/kg every day during protection from light. The PRO (MedChemExpress, USA) was dissolved in PBS at 2 mg/mL, stored at −20°C, and intraperitoneally injected at a dose of 20 mg/kg every day. The femurs of mice were harvested for the detection of NICD^{+} and RUNX2^{+} cells after respective injections of ISO or PRO for 1 week. The femurs of mice were collected after 4 weeks of continuous injection for bone mass analysis and type H vessel assessment.

Micro-CT analysis

For micro-CT analysis, hindlimb bones were collected after sacrificing the mice and then fixed in a 4% polyformaldehyde (PFA) solution (Sigma, USA) overnight at 4°C. The fixed specimens were prepared as 1-cm length segments and scanned using a desktop micro-CT system (eXplore Locus SP, GE Healthcare, USA) with a resolution of 8 μm, voltage of 80 kV, and a current of 80 μA, following previously described methods.[63] Following 3-dimensional image reconstruction, the ROI was selected in the medial metaphysis of the femur. Data analysis was conducted using VGStudio MAX software (Volume Graphics, Germany) and the following trabecular bone parameters were measured as recommended: Tb.BV/TV, Tb.Th, Tb.Sp, Tb.N, Ct.Ar and Ct.Th parameters.[64]

Enzyme-linked immunosorbent assay (ELISA)

To collect bone marrow fluid, the bone marrow cavity was washed multiple times with 200 μL of PBS. The collected fluid was then subjected to centrifugation at 12,000 g for 10 min to collect the supernatant, which was subsequently used for analysis. The concentration of NE (KA1877, Abnova, China) was determined using a commercial ELISA kit.[39]

Immunofluorescent staining

Immunofluorescent staining was performed according to previously published methods.[65] Briefly, fresh femur samples were fixed in 4% PFA (Biosharp, China), decalcified with 17% Ethylene Diamine Tetraacetic Acid (EDTA) decalcification solution (Proandy, China), and dehydrated with 30% sucrose. The femurs were then embedded in an optimal cutting temperature (OCT) compound (Leica, Germany), and 20 μm cryosections were prepared with a cryostat (CM1950, Leica, Germany). The cryosections were permeabilized with 0.3% Triton X-100 (Sigma-Aldrich, USA) for 20 min at room temperature, blocked with goat serum (BOSTER, China) for 30 min at room temperature, and incubated with the primary antibodies overnight at 4°C. The primary antibodies used were anti-CD31 (FAB3628G, R&D Systems, USA; diluted 1:100), anti-EMCN (sc-65495, Santa Cruz Biotechnology, USA; diluted 1:100), anti-TH (ab152, Millipore, USA; diluted 1:100), anti-NICD (3608S, Cell Signaling Technology, USA; diluted 1:100), and anti-RUNX2 (sc-390351, Santa Cruz Biotechnology, USA; diluted 1:100). Following washing with PBS, the cryosections were incubated with fluorescence-conjugated secondary antibodies at room temperature for 1 h. The secondary antibodies used were Cy3-conjugated goat anti-rat IgG (33308ES60, YEASEN, China; diluted 1:200) and Cy5-conjugated goat anti-rabbit IgG (ab6564, Abcam, UK; diluted 1:200). After washing with PBS, the slides were mounted with Mounting Medium With DAPI-aqueous fluoro shield (Abcam, UK).

Confocal laser scanning microscopy (CLSM) (FV1000, Olympus, Japan) was used to capture images, which were analyzed using the ImageJ software (NIH, USA), as we and others previously reported.[36,44,49] Z stacks of high magnification images were scanned at high resolution and were processed and reconstructed in three dimensions with the FV10-ASW Viewer software (Olympus, Japan). Quantification of type H vessel ($CD31^{hi}EMCN^{hi}$) area, type L vessel ($CD31^{lo}EMCN^{lo}$) area, and 20 μm-adjacent areas to type H vessels for TH^+ or $NICD^+$ cell quantification were carried out with ImageJ software. Briefly, ImageJ was used to select the desired regions individually and analyze the proportion (the "density" we refer to) of these areas to the total visual area (% total area), or their respective areas to the region of interest (% ROI). We defined the spatial relationship between TH^+ cells and vessels as "overlap" when positive staining signals were merged. Furthermore, we defined the spatial relationship between TH^+ cells and vessels within a 20-μm range around the vessels, but not merged, as "adjacent". For $NICD^+$ type H vessel quantification, after absolute quantification of the positive $NICD^+CD31^{hi}EMCN^{hi}$ signal area, we performed relative quantification by taking the numerical value of one group as the reference and calculating the relative values of other groups, shown as the fold changes. Each quantification is performed by analyzing three independent regions.

Cell culture and cell experiments

The isolation and culture methods of human umbilical cord-derived MSCs and mouse bone marrow-derived MSCs were previously described.[66] MSCs were cultured with alpha-minimum essential medium (α-MEM, Invitrogen, USA) supplemented with 10% fetal bovine serum (FBS, Sijiqing, China), 2 mM L-glutamine (Invitrogen, USA) and 1% penicillin/streptomycin (Invitrogen, USA) in a humidified atmosphere of 5% CO_2 at 37°C. ECs including human umbilical vein endothelial cells and mouse umbilical vein endothelial cells were purchased from the ATCC and Otwo Biotech and cultured in endothelial cell medium (ECM) (Sciencell, USA) and high glucose Dulbecco's modified Eagle's medium (Hyclone, China) respectively, according to the manufacturer's instructions. For indirect treatment of ECs, the supernatants from MSCs were filtrated at 0.22 μm and mixed with fresh ECM at a 1:1 ratio. The final concentration of ISO treatment for ECs was 100 μM. To determine the formation of a capillary network, an *in vitro* tube formation assay was performed on ibidi μ-Slide angiogenesis dishes (ibidi, Germany) coated with Matrigel (Shanghai NovaMedical Technology, China). ECs were seeded at 2×10^5 cells/mL (50 μL of medium per well) and incubated in the medium without FBS. The specific treatments were the same as described in the migration assay. Tube formation was observed and photographed using an inverted microscope (Leica, Germany) after 5 h. The number of network structures was analyzed by measuring three randomly selected microscopic fields using ImageJ software (NIH, USA). Specific parameters of junctions (points identified as either individual nodes or clusters of fused nodes) and branches (elements delimited by a junction and one extremity) were quantified using the "Angiogenesis Analyzer" for ImageJ software.

Western blot analysis

Western blot analysis was performed following the previously reported protocol.[39] In brief, Cell Lysis Buffer (Beyotime, China) containing protease inhibitor (Roche, Switzerland) was used to prepare cell lysates. Protein quantification was performed using a BCA Protein Assay Kit (TIANGEN, China), and 20 μg of extracted proteins were separated on sodium dodecyl sulfate-polyacrylamide gels and transferred onto polyvinylidene fluoride membranes (Roche, Switzerland). The membranes were blocked with 5% Bovine Serum Albumin (BSA) (MP Biomedicals, USA) for 2 h at room temperature, and then incubated overnight at 4°C with primary antibodies including anti-ADRB1 (A20818, ABclonal, China; diluted 1:1000), anti-ADRB1 (28323-1-AP, Proteintech, China; diluted 1:1000), anti-ADRB2 (A2048, ABclonal, China; diluted 1:1000), anti-ADRB2 (29864, Proteintech, China; diluted 1:1000), anti-ADRB3 (A8607, ABclonal, China; diluted 1:1000), anti-NICD (3608S, Cell Signaling Technology, USA; diluted 1:100), anti-GAPDH (30201ES20, Yeasen, China; diluted 1:1000) and anti-β-Actin (30101ES60, Yeasen, China; diluted 1:1000). Subsequently, the membranes were washed three times with Tris-buffered saline-Tween (TBS-T, Solarbio, China), and then incubated with peroxidase-conjugated secondary antibodies for 1 h at room temperature. The protein bands were visualized using an enhanced chemiluminescence kit (4A Biotech, China) and evaluated using a gel imaging system (4600, Tanon, China). The gray value of protein bands was quantified using ImageJ software (NIH, USA).

mRNA expression analysis

Samples were obtained from cultured cells. Total RNA was extracted from tissues or cells using Trizol Reagent (Takara, Japan) and purified through phenol-chloroform extraction. To synthesize cDNA, RNA was

reverse transcribed using the PCR Amplifier (EasyCycler, German). The primer sequences can be found in Table S1. *GAPDH* and *Actin* were chosen as reference genes for human ECs and mouse ECs respectively. Quantitative real-time PCR (qRT-PCR) was performed using the SYBR Premix Ex Taq II Kit (Takara, Japan) and detected using a Real-Time System (Bio-Rad, USA). For mRNA analysis, the CFX Manager software (Bio-Rad, USA) was utilized.

QUANTIFICATION AND STATISTICAL ANALYSIS

Statistical analysis was performed to determine the significance of the data. The mean and standard deviation (SD) were calculated and presented. Statistical analysis is performed by Student's *t* test for two-group comparison, by one-way analysis of variance followed by Newman-Keuls post-hoc tests for multiple comparisons, or by two-way analysis of variance followed by Sidak's tests for multiple comparisons, with $p < 0.05$ indicating significance (*, $p < 0.05$; **, $p < 0.01$; ***, $p < 0.001$). Graphical and statistical analyses were conducted using GraphPad Prism software (GraphPad Software, USA).